Proc. Lunar Planet. Sci. Conf. 11th (1980), p. 2243–2259.
Printed in the United States of America

A comparison of secondary craters on the Moon, Mercury, and Mars

Peter H. Schultz[1] and Jill Singer[2]

[1]Lunar and Planetary Institute, Houston, Texas 77058 [2]Department of Geological Sciences, Rice University, Houston, Texas 77001

Abstract—Comparison of secondary crater populations around selected martian, lunar and mercurian craters reveals significant differences that are interpreted as the effects of substrate on the cratering flow field and ejecta size. An unnamed 34 km-diameter crater in Chryse Planitia exhibits relative number densities of secondaries comparable to mercurian and lunar craters. Similarly, the maximum extent of the ejecta flow lobes nearly matches the maximum extent (2 crater radii from the rim) of the continuous ejecta facies of similar-size mercurian and lunar craters (adjusted for gravity). In contrast, the crater Arandas (24 km in diameter) exhibits very few secondaries larger than 2% of the primary diameter. The inner ejecta lobe also approximates the continuous ejecta facies of lunar/mercurian craters but the outer lobe extends 4 crater radii from the rim. Arandas secondaries larger than 0.5 km tend to be circular in contrast with secondaries around the Chrysie crater and lunar/mercurian craters. The more circular Arandas secondaries suggest higher ejection angles. Although high ejection angles can reduce the ballistic range and alter the over-all secondary crater distribution, such effects appear not to be sufficient to account for the paucity of Arandas secondaries. The unusual target lithology resulting in high ejection angles also may produce greater fractions of fine-size ejecta. Sufficiently small ejecta will be decelerated by aerodynamic drag and incorporated in near-rim ejecta deposits, rather than forming secondaries. This proposal is consistent with the observed multi-phased sequence of ejecta emplacement for certain martian craters where the outer ejecta lobes have overridden the inner ejecta lobes.

INTRODUCTION

Craters on the Moon, Mars, and Mercury display contrasting styles of ejecta facies that presumably reflect different cratering environments (i.e., gravity, atmosphere, target properties). Two fundamental and distinct problems must be addressed when considering ejecta morphology: ballistic history and ejecta emplacement. On the Moon and Mercury, distinct secondary craters clearly record the effects of the ballistic history. On Mars, ejecta flows reveal the importance of post-ballistic ejecta emplacement, and most discussions have concentrated on this process. Secondary craters also surround martian impact craters, but the Viking images reveal highly variable populations (Carr, *et al.*, 1977; Schultz and

(a)

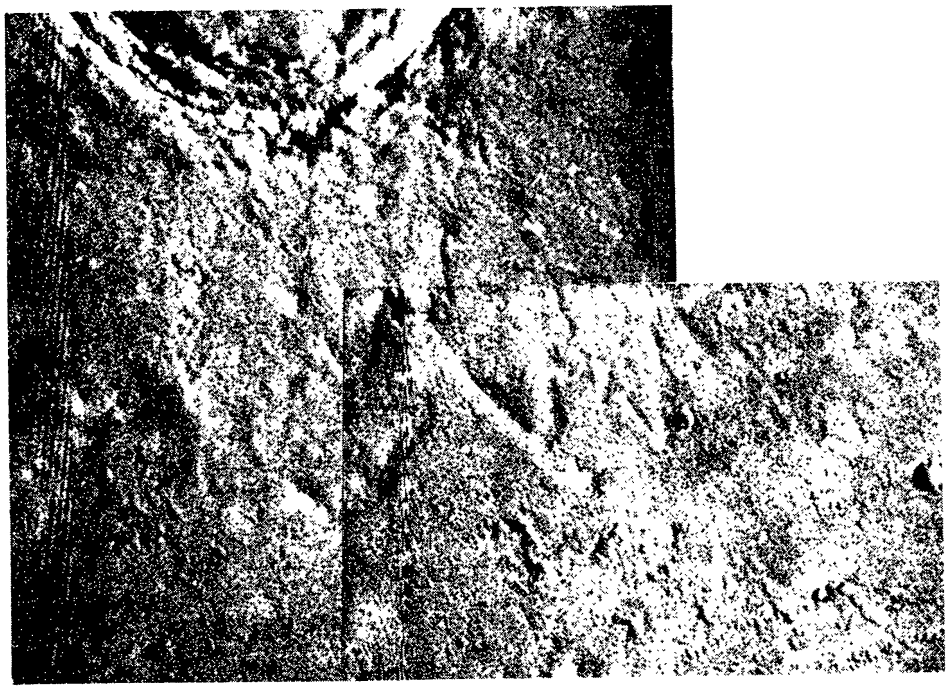

(b)

Fig. 1. Comparison of ejecta facies of selected martian craters. (a) The 24 km-diameter martian crater Arandas situated on the northern fractured plains near latitude +42.8°, longitude 345.1°W. Viking Mosaic 211-5031. Ejecta facies of an unnamed crater (MC-11, Wx; labeled here Crater I) approximately 34 km in diameter in the Chryse Planitia region near latitude +26.5°, longitude 38.8°W. Viking Mosaic 211-5382. (c) Ejecta facies of an unnamed crater (MC-5, Zm; labeled here Crater II) approximately 45 km in diameter situated 600 km northeast of Arandas in the fractured plains near latitude +46.4°, longitude 359.7°W. Viking Mosaic 211-5031.

(c)

Gault, 1979; Mouginis-Mark, 1979a). Previous studies have focused on the existence/absence of secondaries (Mouginis-Mark, 1979b) or on the maximum secondary crater diameter (Allen, 1979). The present study is concerned with the distribution of secondary crater sizes and shapes and the relation of these distributions to inferred martian lithology and ballistic history.

Differences in secondary-crater size/range distributions around unmodified craters can be attributed to differences in gravitational potential, lithologic properties, and atmospheric interactions. All three variables can affect the ballistic range. Material ejected at a given velocity on Mercury and Mars obviously will travel a shorter distance than on the Moon owing to the larger gravitational attraction. Material ejected at high or low angles due to unusual lithologic properties will similarly travel shorter ballistic ranges than material ejected at nominal angles. Finally, sufficiently small ejecta can be aerodynamically decelerated in an atmospheric environment. Consequently, we first compare the size/range distributions of secondaries around selected lunar, mercurian, and martian craters in order to further establish the gravitational effects discussed by Gault *et al.* (1975). Second, we compare the size/range distributions of secondaries around martian craters in different geologic terrains in order to establish possible lithologic effects. These distributions are complemented by measures of circularity that could indicate high or low ejection angles. Third, we make first-order corrections for gravity and ejection angles in order to evaluate whether or not the last variable (atmospheric effects) must be considered. Finally, we consider complementary morphologic evidence for separation of the variables.

DATA SET

Primary craters were selected on the basis of crater size, inferred target lithology, available resolution, and completeness of coverage. As previous studies have shown (Carr, *et al.*, 1977; Schultz and Gault, 1979; Mouginis-Mark, 1979b), the complexity of ejecta facies on Mars increases with increasing crater size. Ejecta facies of craters smaller than about 1 km–3 km in diameter typically resemble lunar craters. Ejecta facies of martian craters between 5 km and 50 km exhibit clear evidence for flow expressed as rampart-bordered and multi-lobed deposits with highly variable secondary crater populations. Ejecta facies of craters larger than 50 km typically are highly complex and composed of extensive secondary crater populations with multiple and overlapping ejecta flow lobes. The intermediate size range (5 km–50 km) was selected because of the diversity in emplacement style. Although this size range could be applied easily to the Moon, equivalent size craters on Mercury could not be selected, owing to resolutions that were insufficient for clear identification of secondaries.

Three martian craters smaller than 50 km in diameter were selected on the basis of contrasting inferred target lithologies and completeness of coverage at sufficient resolutions. The crater Arandas (24 km in diameter) occurs in the northern fractured plains and is surrounded by an extensive multi-lobed ejecta deposit (Fig. 1). The fractured plains are interpreted as regions of high water-ice content analogous to terrestrial patterned ground (Carr and Schaber, 1977). Viking coverage of this region permits resolving secondary craters as small as 0.2 km in diameter in two 180° sectors out to 6 crater radii from the primary-crater center and in two 30° sectors beyond 10 crater radii.

A 34-km diameter crater in Chryse Planitia displays markedly different ejecta facies (Fig. 1b) dominated by secondary craters in the outer deposits with multi-lobed ejecta flows in the inner deposits. The crater is designated as Crater Wx in MC-11 (see Batson *et al.*, 1979), but is denoted as Crater I in this paper. The Chryse plains are interpreted as basalt surfaces partly mantled by aeolian and outwash materials (Greeley, *et al.*, 1977; Theilig and Greeley, 1979). Contiguous Viking coverage of Crater I permits resolving 0.2 km diameter secondaries within a 120° sector out to 8 crater radii, and within a 30° sector beyond 12 crater radii.

An additional but larger crater (Fig. 1c) approximately 45 km in diameter was selected in the fractured plains region 600 km northeast of Arandas (Crater Zm in MC-5 but denoted here as Crater II). This additional crater was selected, since the large number of secondaries around Crater I relative to Arandas might be attributed to its slightly larger size rather than differences in target lithology. Contiguous Viking coverage of Crater II allows resolving 0.2 km-diameter secondaries within a 180° sector out to 10 crater radii, and within a 30° sector beyond 12 crater radii.

The craters Aristarchus (39 km; Fig. 2b) and Copernicus (96 km; Fig. 2a) comprise the lunar data set. Copernicus is significantly larger than the selected martian craters, but owing to the difference in gravity, the impact velocity of ejecta at a given *relative* range approximates the impact velocity of ejecta from a 50 km diameter martian crater. Ejecta velocities around Aristarchus approximate velocities from smaller martian craters comparable in size to Arandas.

Selection of an appropriate mercurian crater was hampered by incomplete coverage at sufficiently high resolutions. In order to assess the secondary crater populations to relative ranges of 7 crater radii, a primary crater significantly larger than the selected craters on Mars was considered. Nevertheless, these data provide a useful comparison. Mariner 10 images of the crater Alencar (110 km; Fig. 3) permit measurements nearly 180° in azimuth, but topography and another major crater in one sector limits useful data out to 5 crater radii within a 90° sector and 7 crater radii within a 30° sector.

Secondary craters were identified on the basis of occurrence as chains or clusters or as members of a crater ray. By lunar analogy, other characteristics included elongate or irregular plan, shallow profile, subdued morphology, and the herringbone pattern. These characteristics eliminate certain types of secondary craters, but represent consistent criteria. Because of the wide range in available resolutions, only secondaries larger than 1–2% of the primary crater diameter were recorded. The distinguishing characteristics of secondaries become less pronounced at large distances from the primary (>12 R) and can be confused with secondaries from other craters. Consequently, limiting resolutions also prevented confident identification of secondaries for a given primary at large ranges.

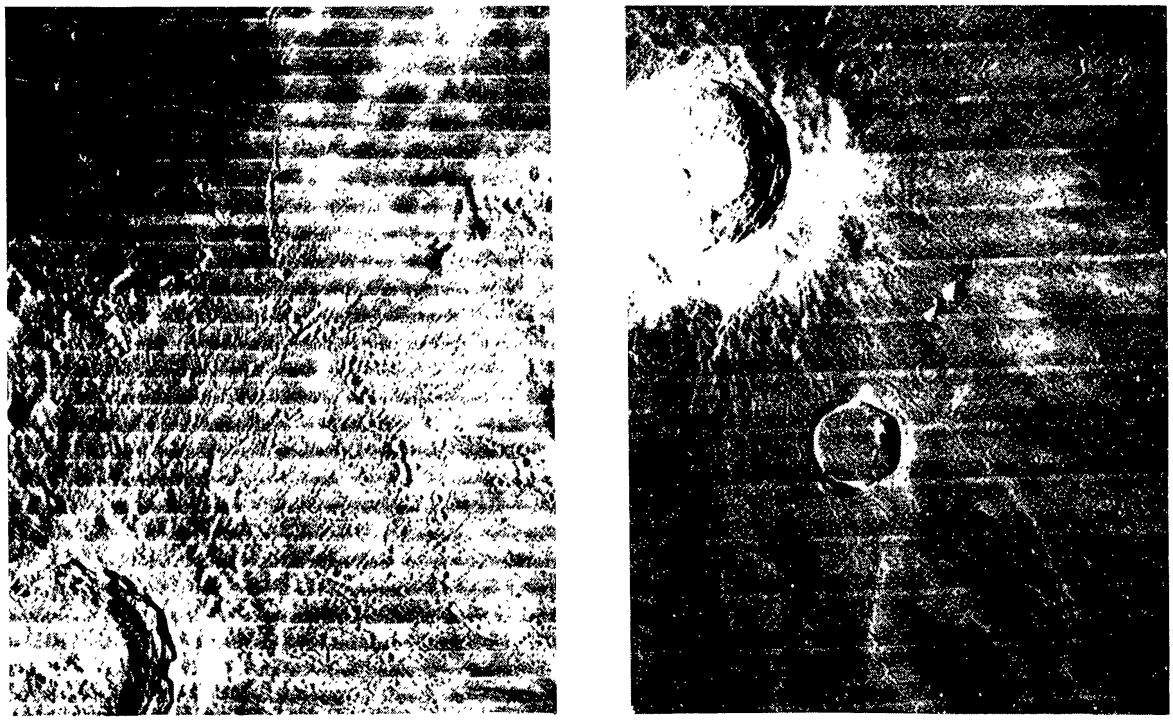

(a) (b)

Fig. 2. Comparison of ejecta facies of selected lunar craters. (a) The lunar crater Copernicus (96 km) near latitude +9.7°, 19.9°W. Lunar Orbiter IV-121-H2. (b) The lunar crater Aristarchus (39 km) near latitude +23.7°, longitude 47.4°W. Lunar Orbiter IV-150-H3.

RESULTS

The distribution of secondary craters through a complete 360° azimuth could not be obtained for all craters owing to incomplete coverage, overlapping secondary crater fields, insufficient resolution, and contrasting resolutions dependent on terrain. Consequently, the collected data were analyzed within 30° arc sectors where the most consistent data could be obtained to the farthest distance from the primary. Comparison of different azimuth sectors of the same crater provides a check for any gross asymmetries in the secondary crater populations.

Figures 4 and 5 permit comparison of the raw data and include the approximate limits of the continuous ejecta deposits. The continuous ejecta facies (CEF) of the mercurian crater Alencar (Fig. 4) extends to about 1.8 R from the crater center in contrast to 2.3 R and 3 R for the lunar craters Copernicus and Aristarchus, respectively. The minimum extent of the ejecta flow lobe of Crater I (Chryse Planitia, Fig. 5) approximates the limit of the mercurian ejecta facies (2 R), and the maximum extent of both the inner lobe and the outer lobe of Crater I extends to about 3 R (2.8 R and 3.1 R, respectively). Data from Gault *et al.* (1975) as well as Fig. 4, indicate that the extent of the continuous ejecta facies increases with decreasing crater size. Consequently, the extent of the multiple lobes of Crater I on Mars is not significantly different from the limit of the

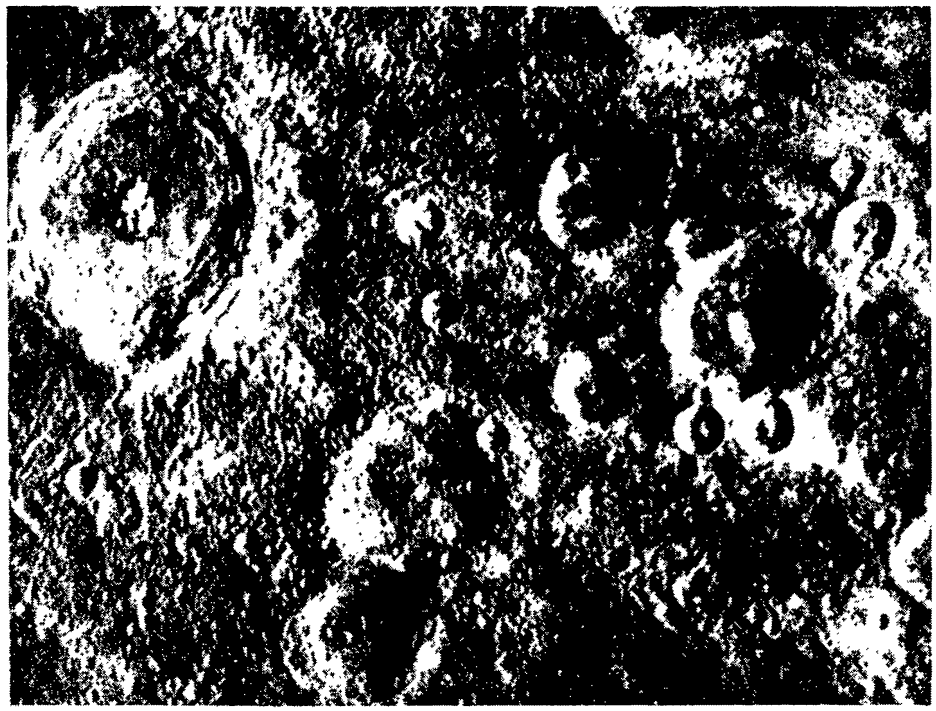

Fig. 3. The mercurian crater Alencar (110 km) near latitude −63.3°, longitude 104.0°W. FDS 166727.

continuous ejecta facies for a crater on Mercury. Similarly, the extent of the thick, inner ejecta lobes of Arandas approximate the continuous ejecta facies of a mercurian crater of comparable size. The inner lobes of Crater II are not easily delineated, as is characteristic of larger multi-lobed martian craters (Schultz and Gault, 1979; Mouginis-Mark, 1979a). In contrast, the outer ejecta lobes of both Crater II and Arandas extend to about 5 R.

Secondary craters become prominent beyond the limit of the continuous ejecta facies for Alencar, Copernicus, and Aristarchus. Although subdued depressions within these deposits are also probable secondaries, they are not always identifiable if lighting conditions are not favorable. Figure 4b shows that the large number of secondaries around these lunar/mercurian craters are matched by martian Crater I (Chryse Planitia). Crater II and Arandas, however, are generally devoid of secondaries. Secondaries occur within the ejecta lobes of Crater II, but generally appear to be overridden or surrounded by the relatively thin ejecta lobe. Arandas secondaries larger than 2% of the primary diameter are relatively rare, even beyond the outer limit of the ejecta flow lobes. This paucity of secondaries is confirmed in other azimuth sectors.

Figure 5 allows comparison of secondary crater frequency within the same relative areas (annuli) at different ranges from the crater center. This representation normalizes the secondary crater population within each annulus to the crater size and permits direct comparison of the number of secondary craters produced by different size primary craters. Figure 5 shows that the *relative* areal

density of secondary craters for Copernicus and Aristarchus are nearly the same. It should be remembered, however, that the *absolute* number of secondaries around Aristarchus is significantly less than the number around Copernicus. The absence of secondaries between the rim and 2 R from the rim of Aristarchus is largely due to the larger extent of its continuous ejecta facies, as noted in Fig. 4a. There are significantly fewer secondaries between 3 R and 4 R for Copernicus than for Aristarchus. Shoemaker (1962) noted a similar deficiency and attributed it to confusion with Eratosthenian secondaries and lighting conditions for the terrestrial view used. Although lighting limitations are not a problem with Lunar

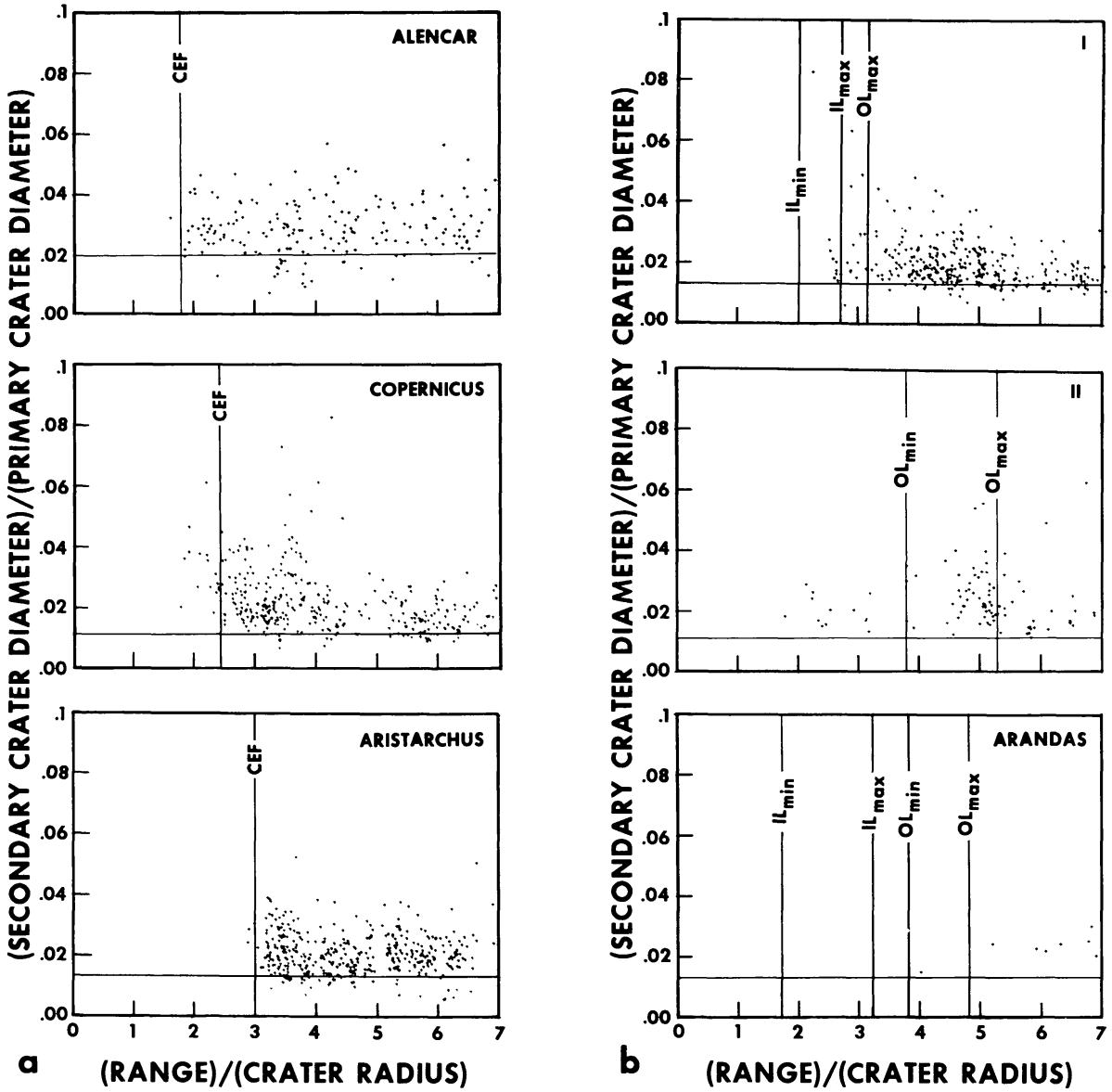

Fig. 4. Comparison of secondary crater size distributions within a 30° sector. (a) Craters Alencar (Mercury), Copernicus (Moon), and Aristarchus (Moon). The limit of the continuous ejecta facies is indicated by CEF. (b) The martian craters, Crater I, Crater II, and Arandas (see Fig. 2). The minimum and maximum extents of the inner (IL) and outer (OL) flow lobes are indicated.

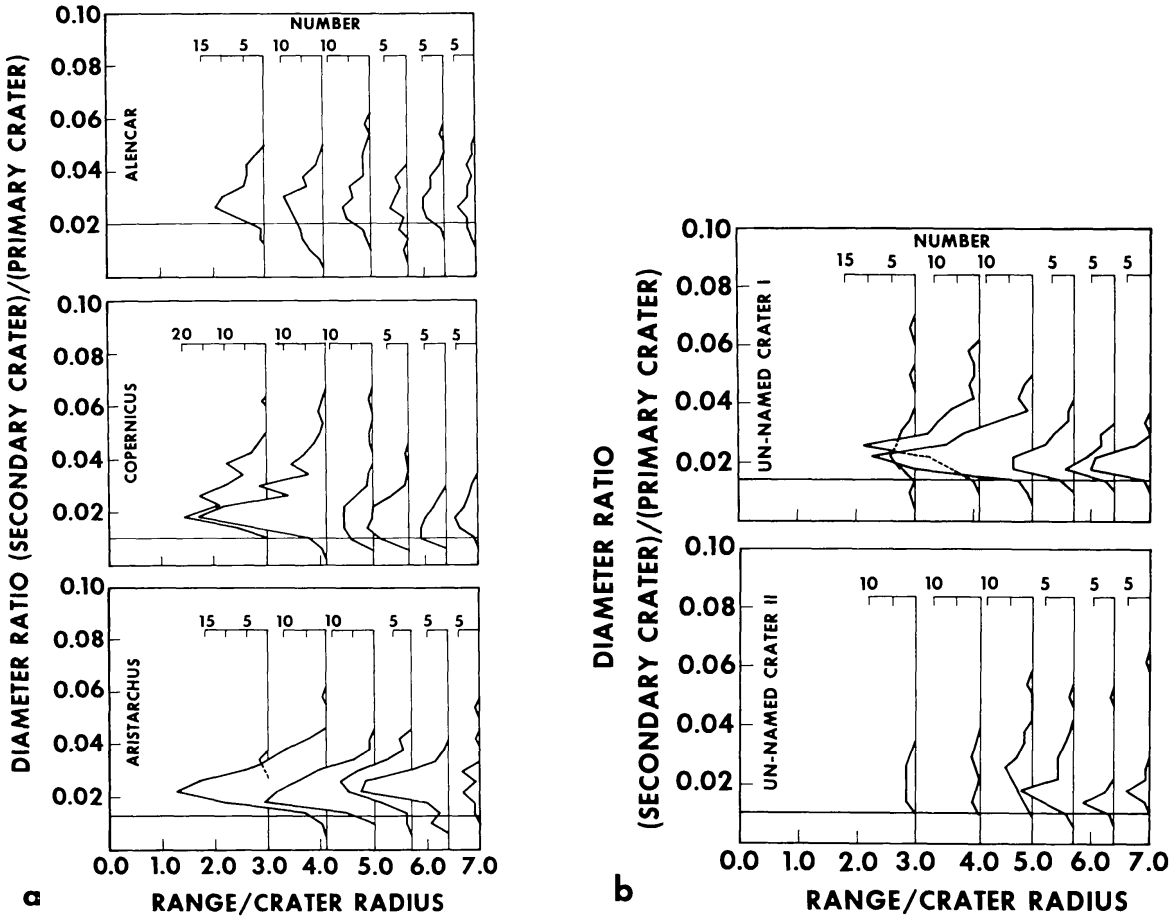

Fig. 5. The size-frequency distribution of secondaries within the same relative areas of different craters within 30° sectors. The horizontal lines indicate the approximate resolution cut-off of the collected data. The crater Arandas is not illustrated owing to the few secondaries counted above the resolution cut-off.

Orbiter photography of this region, secondaries from Eratosthenes complicate consistent identification of Copernican secondaries. The reduced number of secondaries within 5 R for the mercurian crater Alencar reflects the difficulty in clearly identifying secondaries in the more rugged terrains. Although the theoretical resolution is normally quoted as 2.2 pixels (Saunders *et al.*, 1975), practical resolution is dependent on terrain and is significantly poorer. In rugged terrains, as many as 90% of the craters 2.2 pixels in diameter are unidentified (Schultz, 1977).

Figure 5b confirms the similarity in the secondary crater distributions between Crater I and the lunar and mercurian craters, whereas Crater II displays a notable deficiency. The crater Arandas (not included in Fig. 5b) has even fewer secondaries, as shown in Fig. 4b.

Short and long axes of each secondary crater were measured and rectified, thereby permitting a measure of circularity. Figure 6 reveals that Alencar, Copernicus, Aristarchus, and Crater I have secondaries with wide ranges in circularity: values of short/long axes typically near 0.78, 0.8, 0.7, and 0.6, respectively.

In contrast, the identified secondaries of Arandas generally are highly circular (0.9) within 8 R and show lower circularity beyond 8 R. Smaller secondaries (not included in the data), however, have more elongate plans. Secondaries associated with Crater II are also more circular (0.8) than those around Crater I, but clearly more elongate or irregular than secondaries associated with Arandas.

DISCUSSION

Five parameters affect the size distribution of secondary craters: gravitational potential, ejection angle, ejection velocity, ejecta size, and ejecta state (solid, dispersed). Gault, *et al.* (1975) showed that the secondary crater population is not appreciably different beyond the region of continuous ejecta for the Moon and Mercury. Figure 5 indicates that Crater I in Chryse Planitia on Mars is also similar. The distribution of secondaries around Copernicus and Aristarchus can be adjusted simply for the gravity of Mars and compared with Crater I. Figure 7 reveals that such a correction most notably affects the near-rim distribution of secondaries, as observed by Gault *et al.* (1975). Secondaries at large ranges are pulled closer to the rim and increase this population without drastically modifying the overall distribution. Crater I exhibits a distribution very similar to the gravity-

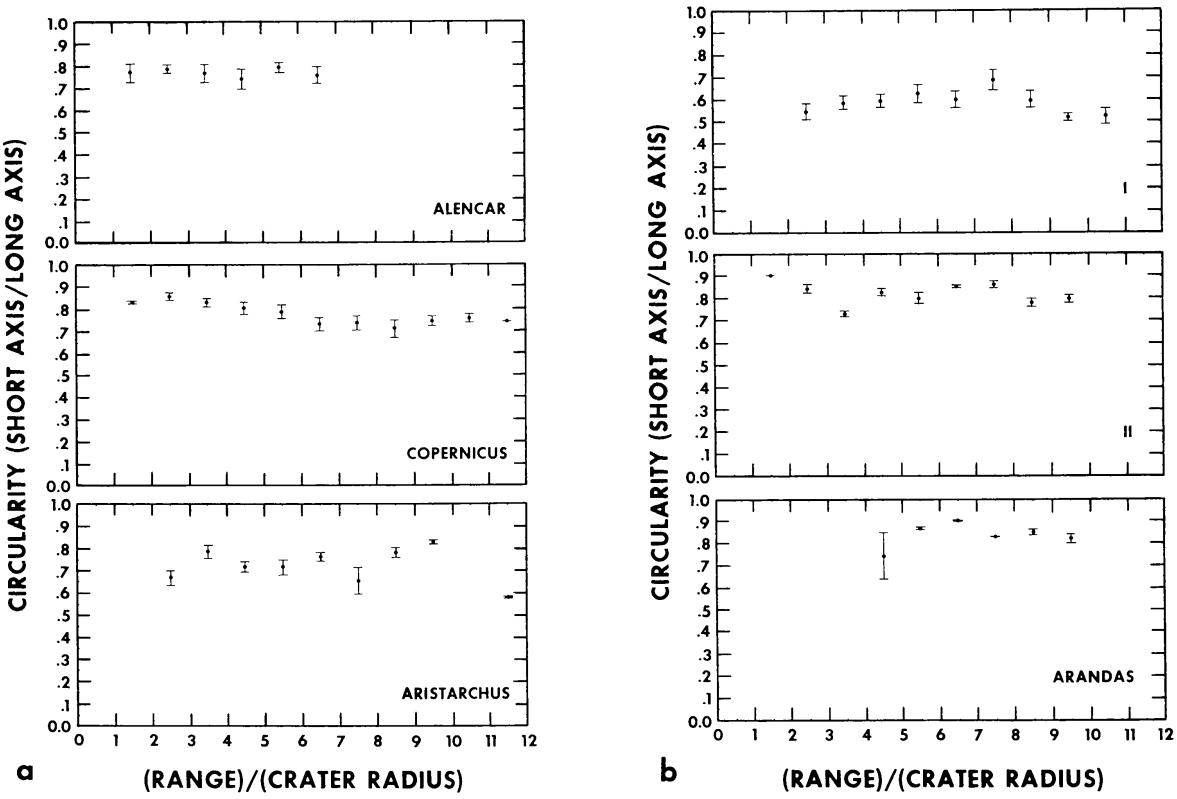

Fig. 6. The mean circularity of all measured secondary craters at different ranges for different craters. The error bars represent a one standard-deviation statistical spread of the data. The large deviation for Arandas near 4 R indicates the paucity rather than statistical spread of the data.

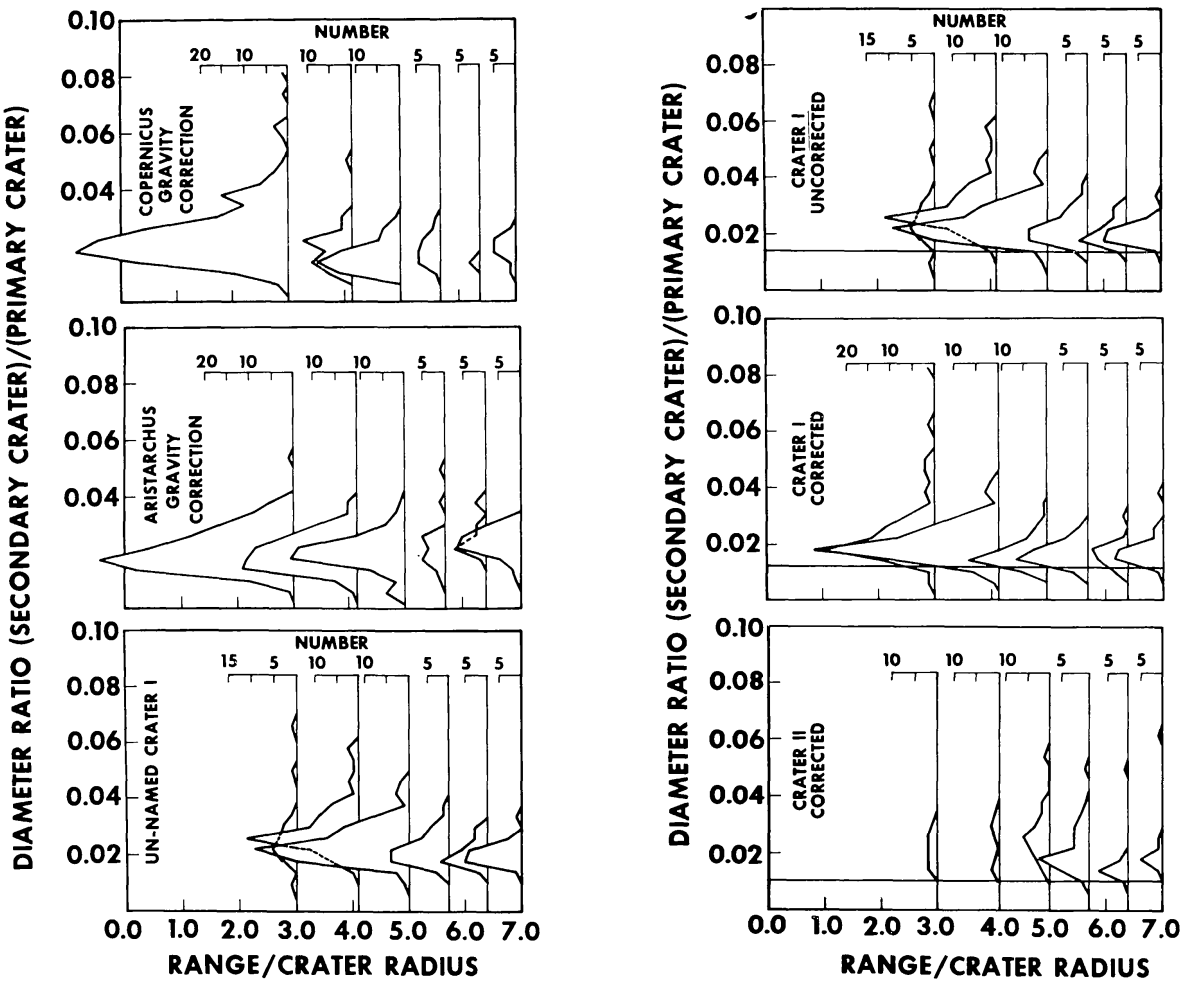

Fig. 7. The size-frequency distribution of secondaries within the same relative areas for Copernicus and Aristarchus after the observed range of secondaries (Fig. 4a) was reduced to match conditions of martian gravity. The large number of secondaries within 2 R of the rim would be represented by the continuous ejecta facies. Crater I in Chryse Planitia on Mars shows a similar size-frequency distribution beyond the multi-lobed ejecta flows.

Fig. 8. Comparison of the size-frequency distribution of secondaries within the same relative areas for martian Crater I before (top) and after (middle) reduction of range due to increasing the assumed ejection angle from 45° to 75°. As in Fig. 7, the most pronounced change occurs near the rim and may contribute to the massive ejecta flows developed around certain martian craters. Increased ejection angles may not account completely for the few craters beyond the multiple ejecta lobes of Crater II and are even less likely to account for the relative absence of secondaries around Arandas (Fig. 4b).

adjusted distributions for the lunar craters, except within the ejecta flow lobes, which incorporated or buried the near-rim secondaries. The paucity of secondaries around Crater II and Arandas, therefore, suggests the influence of parameters other than gravity.

Gault and Greeley (1978) and Greeley *et al.* (1980) demonstrated that impacts in low-viscosity targets eject material at appreciably higher ejection angles from the horizontal than impacts in high-viscosity targets. Thomsen *et al.* (1979; 1980)

confirmed this for different material of low viscosity and calculated a similar crater flow field. Different ejection angles theoretically affect both the distribution of secondaries with distance from the primary and the size of the secondary. High (or very low) ejection angles will reduce the ballistic range for the same ejection velocity, thereby influencing the spatial distribution of secondaries. Gault (1974) notes that crater size increases as the impact angle increases according to $(\sin \theta)^{1/3}$. Consequently, an increased impact angle (and, at the same range, an increased velocity) would also be expected to increase secondary crater size, an effect that should increase the observed population of secondaries as they are raised above the resolution cut-off. For example, at 6 R from Arandas an ejection angle of 75° rather than 45° would increase the size 66%: 37% due to the increased ejection angle and 21% due to the increased velocity required to achieve the same ballistic range.

If the observed secondaries around Crater I were produced by ejecta with an ejection angle of 45° (producing the maximum ballistic range), then an ejection angle of 75° would reduce the range by a factor of two for the same ejection velocity. Such a range reduction applied to Crater I produces the distribution shown in Fig. 8. This reduction is insufficient to produce the deficiency of secondaries associated with Crater II and even less effective for secondaries of Arandas. Therefore, high ejection angles alone perhaps cannot account for the few secondaries associated with Arandas and Crater II. It should be noted, however, that the velocity flow fields in two contrasting media are only beginning to be addressed (Greeley *et al.*, 1980; Thomsen *et al.*, 1980; Austin *et al.*, 1980), and the assumption that the vector velocities of ejecta are the same is most likely in error. More detailed theoretical and experimental studies are clearly required.

The greater circularity for secondaries of Arandas (Fig. 6) supports the contention that ejection angles were higher than those for Crater I, Aristarchus, Copernicus, and Alencar. Consequently, suggestions that the target material in this region of Mars exhibited a low yield strength at the time of formation (Carr *et al.*, 1976; Gault and Greeley, 1978; Boyce, 1979; Schultz and Gault, 1979; Greeley *et al.*, 1980) gain further support. However, the few Arandas secondaries of sufficient size to be included in this study require further discussion.

Ejecta size and physical state also can affect the formation of secondary craters. Ejecta below a critical size can be decelerated by aerodynamic drag, thereby reducing the ballistic range and incorporating this fraction in a late-stage, near-rim ejecta deposit (Schultz and Gault, 1979). For Arandas-size craters this critical size is about 10 cm. If the pre-impact target lithology contains large amounts of water or ice, shock vaporization of this component may lead to increased comminution. Moreover, the dynamic forces should disperse any liquid ejecta and result in a low-density cloud of atomized liquid and solids traveling in close proximity, rather than a single ejecta block. If massive enough, such an impacting system may form detached fluidized ejecta deposits (Greeley *et al.*, 1980). If the velocity is high enough, craters with mounded floors may be formed (Schultz *et al.*, 1980). Highly dispersed ejecta, however, will not penetrate the surface to great depths and will scour the surface without producing large secondary craters.

The few secondaries around Arandas illustrated in Fig. 4b, therefore, may

have three causes: little mass arriving beyond the ejecta flow lobes; dispersed small-size ejecta (but above the critical particle size) not forming identifiable secondary craters; and/or ejecta configurations producing deposits and secondaries that do not fit within the selection criteria used in this study. The first possibility results from high ejection angles, lower relative velocities, and aerodynamic effects on small-size ejecta. The combination of these factors can result in late-arriving ejecta that override early-arriving ejecta, which comprise the massive overturned flap of smaller craters (Schultz and Gault, 1979). Figure 9 illustrates a 20 km-diameter crater in Elysium Planitia region of Mars (+35°, 211°) where grooves and ridges continuously cross the inner lobe of ejecta deposits and extend through the outer lobe. This morphology is not unique and is consistent with a scouring action by late-arriving ejecta materials, perhaps analogous to a base surge. A similar sequence has been proposed for Arandas (Mouginis-Mark, 1980).

The second possible cause of missing secondaries involves small-size but undecelerated ejecta. Faint ray systems extend from Arandas (Fig. 10a) and other martian craters. Occurrence of ray systems indicates that high-velocity, small-

Fig. 9. Martian crater (MC-7, Nd; 20 km diameter) near latitude +35°, longitude 211°W that exhibits radial grooves (arrow) and ridges extending across inner, thick ejecta lobe onto the outer ejecta lobe. This sequence of emplacement suggests a late-stage flow of ejecta overriding the inner lobe. Viking Frame 86A14.

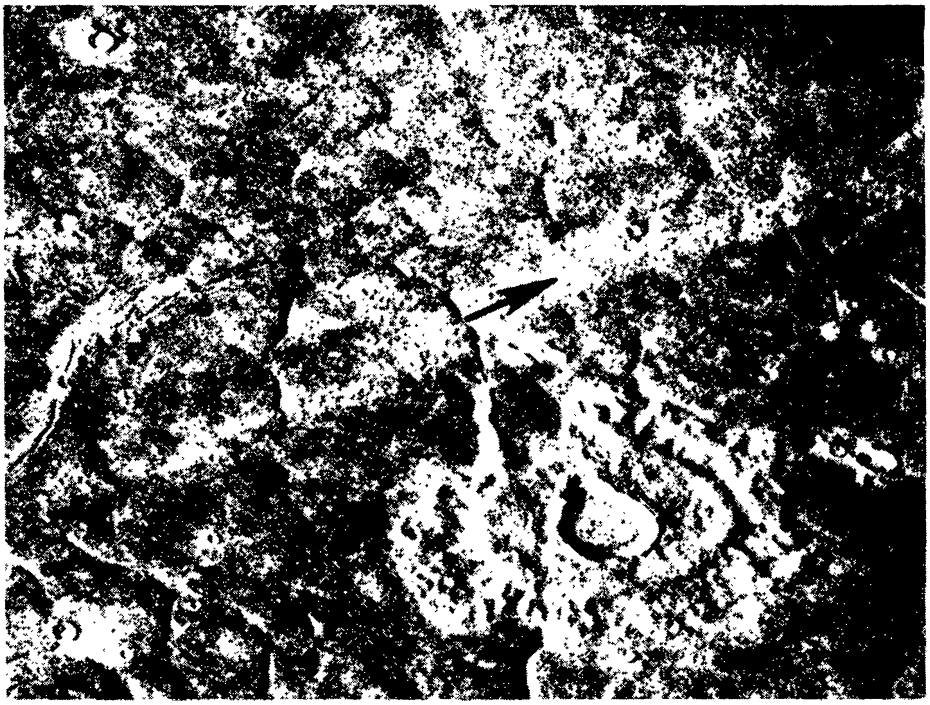

(a)

(b)

Fig. 10. The martian crater Arandas. (a) Ray system composed of small (<0.5 km) secondary craters below the size limit used in this study. Such rays were formed by ejecta large enough to be unaffected by aerodynamic drag, but small enough to produce barely recognizeable secondary craters. Area shown is approximately 30 km across. Viking Frame 32A21. (b) Hummocky units probably associated with Arandas and representing detached segments of ejecta deposits. Such units also are not included in the statistics but may represent low velocity, viscous ejecta or recocheted pieces of the ejecta flow lobes from the continuous facies. Viking Frame 32A32.

size ejecta extend to significant ranges without forming secondaries large enough to be included in this study. In addition, numerous secondaries can be identified beyond the ejecta lobes of Arandas, but are below our size-selection criterion. Many of these secondaries appear to be more elongate than the larger secondaries; therefore, they may indicate a high-velocity, low ejection-angle component of the ejecta.

The third cause is best illustrated by hillocky deposits radial to Arandas, but separated from the ejecta flow lobes (Fig. 10b). Secondary craters commonly are not associated with these deposits, yet the association with Arandas is unmistakable. They may be related to groups of dispersed fluidized ejecta that did not form secondary craters, but coalesced at impact to produce a limited flow separated from the main lobe as observed in the laboratory (Gault and Greeley, 1978; Greeley *et al.*, 1980). Alternatively, they may represent lower velocity fluidized segments recocheted and detached from the uprange ejecta lobe.

Figure 11a illustrates a type of crater not classed as a secondary crater, yet might be one. Such secondaries typically are circular with a diffuse halo and a central mound. A central mound has been recognized for certain lunar secondaries (Schultz and Mendenhall, 1979) and has been reproduced in the laboratory by impacting systems and fluidized and dispersed ejecta (Schultz and Mendenhall, 1979; Schultz *et al.*, 1980). The possibility of widely dispersed ejecta groups is illustrated by secondary crater clusters and chains. A more tightly clustered system perhaps associated with Arandas is shown in Fig. 11b.

CONCLUDING REMARKS

Although the number of primary craters used in this study is small, the results nevertheless have implications for interpreting the statistics of martian crater morphologies on a global scale. The following major points can be summarized:

1. The similarity in the distribution of secondaries and in the extent of the continuous ejecta facies between Crater I on Mars and craters of similar size on Mercury suggests that neither atmospheric nor target effects drastically modified the radial distribution of ejecta for certain martian craters.
2. Although numerous martian impact craters have major differences in the morphology and maximum extent of the ejecta flow lobes, the inner flow lobe of Arandas and other multi-lobed craters extends to about the same relative distance (2 R) as the continuous ejecta facies of similar-size mercurian craters.
3. Two craters with extensive flow lobes in the fractured plains region have very few secondaries larger than 2% the diameter of the primary.
4. Secondary craters associated with two multi-lobed craters in the fractured plains are significantly more circular than secondaries associated with a crater in the Chryse Planitia as well as secondaries around lunar and mercurian craters.

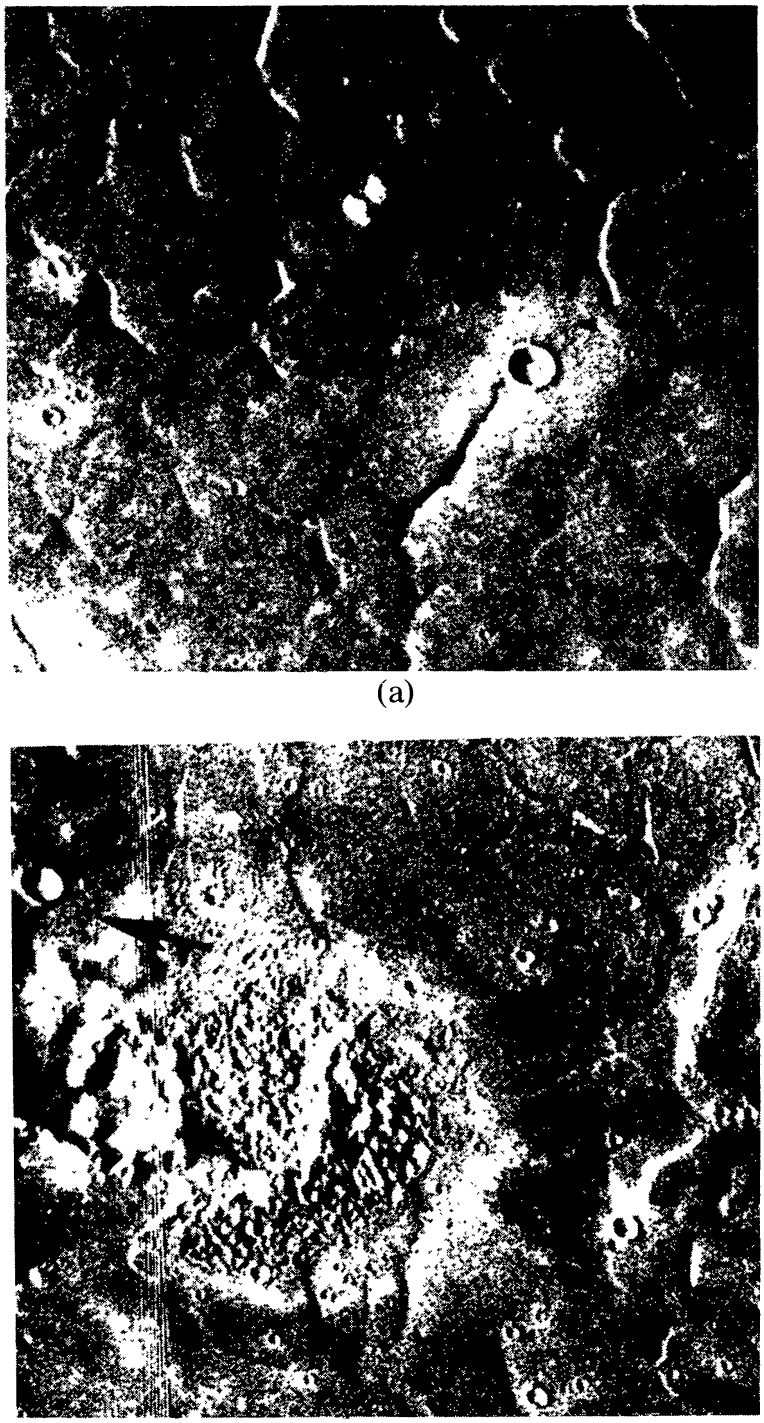

(a)

(b)

Fig. 11. Possible Arandas secondary craters. (a) Small (2 km) mounded-floor crater that could have developed by low velocity impacts (characteristic of secondary craters) by low viscosity projectiles. Such craters were not included in the statistics shown in Fig. 4. Viking Frame 32A35. (b) A tight cluster of small (<1 km) craters interpreted as secondaries from Arandas (direction indicated by arrow). Diffuse bright halo (15 km across) is slightly asymmetric, extending away from Arandas. The symmetry of this tertiary ejecta halo is in contrast to secondary craters on the Moon and further supports high angle ejection and impact of primary ejecta. Viking Frame 32A35.

5. Simple models correcting for possible high ejection angles do not appear to account for the paucity of secondaries beyond the outer ejecta flow lobes of Arandas.
6. The outer ejecta lobe of certain multi-lobe impact craters appear to have overridden the inner ejecta lobe.

The wide variations in secondary crater populations around medium-size (5–50 km) martian craters can be interpreted as effects of contrasting target lithologies. The extensive secondary cratering and elongate secondaries of Crater I in Chryse Planitia are consistent with a competent lithology of basaltic plains, as inferred from various photogeologic studies (e.g., Greeley *et al.*, 1977). Such targets would be expected to have relatively large ejecta, and experiments (Gault and Heitowit, 1963) indicate relatively low ejection angles (<50°). The relatively few large secondaries around Arandas, and their high circularity, are consistent with a lithology exhibiting low yield strength, as inferred for the fractured plains (e.g., Carr and Schaber, 1977). Here ejecta sizes probably are small owing to pre-impact grain size and enhanced comminution. The high ejection angles shown in experiments will contribute to a more massive near-rim arrival of ejecta (Gault and Greeley, 1978; Schultz and Gault, 1979; Greeley *et al.*, 1980). Aerodynamically decelerated fine-size ejecta will enhance near-rim arrival and could result in a late-stage flow overriding the inner ejecta flow lobes and forming or enhancing the outer flow lobes (Schultz and Gault, 1979; Mouginis-Mark, 1980).

Acknowledgments—The authors appreciate the detailed reviews by D. Wilhelms and C. Wood. Jill Singer gratefully acknowledges participation in the LPI Summer Intern Program. We also greatly appreciate the computer programming of John Harvey and Kin Leung. The Lunar and Planetary Institute is operated by the Universities Space Research Association under Contract No. NSR 09-051-001 with the National Aeronautics and Space Administration. This paper constitutes the Lunar and Planetary Institute Contribution No. 418.

REFERENCES

Allen C. C. (1979) Large lunar secondary craters: Size-range relationships. *Geophys. Res. Lett.* **6,** 51–54.

Austin M. G., Thomsen J. M., Ruhl S. F., Orphal D. L., and Schultz P. H. (1980 Calculational investigation of impact cratering dynamics: Material motions during the crater growth period. *Proc. Lunar Planet. Sci. Conf. 11th*. This volume.

Batson R. M., Bridges P. M., and Inge J. L. (1979) *Atlas of Mars*. NASA SP-48. 146 pp.

Boyce J. M. (1979) A method for measuring heat flow in the martian crust using impact crater morphology. Reports of Planetary Geology Program 1978–1979, p. 114–118. NASA TM-80339.

Carr M. H., Crumpler J. A., Cutts R., Greeley R., Guest J. E., and Masursky H. (1977) Martian impact craters and emplacement of ejecta by surface flow. *J. Geophys. Res.* **82,** 4055–4065.

Carr M. H. and Schaber G. G. (1977) Martian permafrost features. *J. Geophys. Res.* **82,** 4039–4054.

Gault D. E. (1974) Impact cratering. In *A Primer in Lunar Geology* (R. Greeley and P. Schultz, eds.), p. 137–176. TM X-62359.

Gault D. E. and Greeley R. (1978) Exploratory experiments of impact craters formed in viscous-liquid targets: analogs for rampart craters? *Icarus* **34,** 386–495.

Gault D. E., Guest J. E., Murray J. B., Dzurisin D., and Malin M. C. (1975) Some comparisons of impact craters on Mercury and the Moon. *J. Geophys. Res.* **80,** 2444–2460.

Gault D. E. and E. D. Heitowit (1963) The partitioning of energy for hypervelocity impact craters formed in rock. *Proc. 6th Symposium on Hypervelocity Impact,* p. 419–456.

Greeley R., Fink J., Gault D. E., Snyder D. B., Guest J. E., and Schultz P. H. (1980). Impact cratering in viscous targets: Laboratory experiments. *Proc. Lunar Planet. Sci. Conf. 11th.* This volume.

Greeley R. Theilig E., Guest J. E., Carr M. H., Masursky H., and Cutts J. A. (1977) Geology of Chryse Planitia. *J. Geophys. Res.* **82,** 4093–4109.

Mouginis-Mark P. (1979a) Ejecta emplacement of the martian impact crater Bamburg. *Proc. Lunar Planet. Sci. Conf. 10th,* p. 2651–2668.

Mouginis-Mark P. (1979b) Martian fluidized crater morphology: variations with crater size, latitude, altitude, and target material. *J. Geophys. Res.* **82,** 8011–8022.

Mouginis-Mark P. (1980) An emplacement sequence for martian fluidized ejecta craters (abstract). In *Lunar and Planetary Science XI,* p. 753–755. Lunar and Planetary Institute, Houston.

Saunders R. S., Mutch T. A., and Jones K. L. (1975) Guide to the use of Mariner images. *JPL Tech. Mem. 33–723.* 27 pp.

Schultz P. H. (1977) Endogenic modification of impact craters on Mercury. *Phys. Earth Planet. Inter.* **15,** 202–219.

Schultz P. H. and Gault D. E. (1979) Atmospheric effects on martian ejecta emplacement. *J. Geophys. Res.* **84,** 7669–7687.

Schultz P. H., Gault D. E., and Mendenhall M. H. (1980) Multiple-body impacts: implications for secondary impact processes (abstract). In *Lunar and Planetary Science XI,* p. 1006–1008. Lunar and Planetary Institute, Houston.

Schultz P. H. and Mendenhall M. H. (1979) On the formation of basin secondary craters by ejecta complexes (abstract). In *Lunar and Planetary Science X,* p. 1078–1080. Lunar and Planetary Institute, Houston.

Shoemaker E. M. (1962) Interpretation of lunar craters. In *Physics and Astronomy of the Moon* (Z. Kopal, ed.), p. 283–359. Academic, N.Y.

Theilig E. and Greeley R. (1979) Plains and channels in the Lunae Planum-Chryse Planitia region of Mars. *J. Geophys. Res.* **84,** 7994–8010.

Thomsen J. M., Austin M. G., Ruhl S. F., Schultz P. H. and Orphal D. L. (1979) Calculational investigation of impact cratering dynamics: early time material motions. *Proc. Lunar Planet. Sci. Conf. 10th,* p. 2741–2756.

Thomsen J. M., Austin M. G., Schultz P. H. (1980) The development of the ejecta plume in a laboratory-scale impact cratering event (abstract). In *Lunar and Planetary Science XI,* p. 1146–1148. Lunar and Planetary Institute, Houston.